Anisotropies and what we can learn from them

1. Recent Observations
2. Anisotropies: general considerations
3. Modelling Cosmic Rays in the Structured Universe

Deutsche Forschungsgemeinschaft

PROJEKTTRÄGER FÜR DAS Bundesministerium für Bildung und Forschung

Universität Hamburg
DER FORSCHUNG | DER LEHRE | DER BILDUNG

Günter Sigl
II. Institut theoretische Physik, Universität Hamburg

Newest Results on Anisotropy

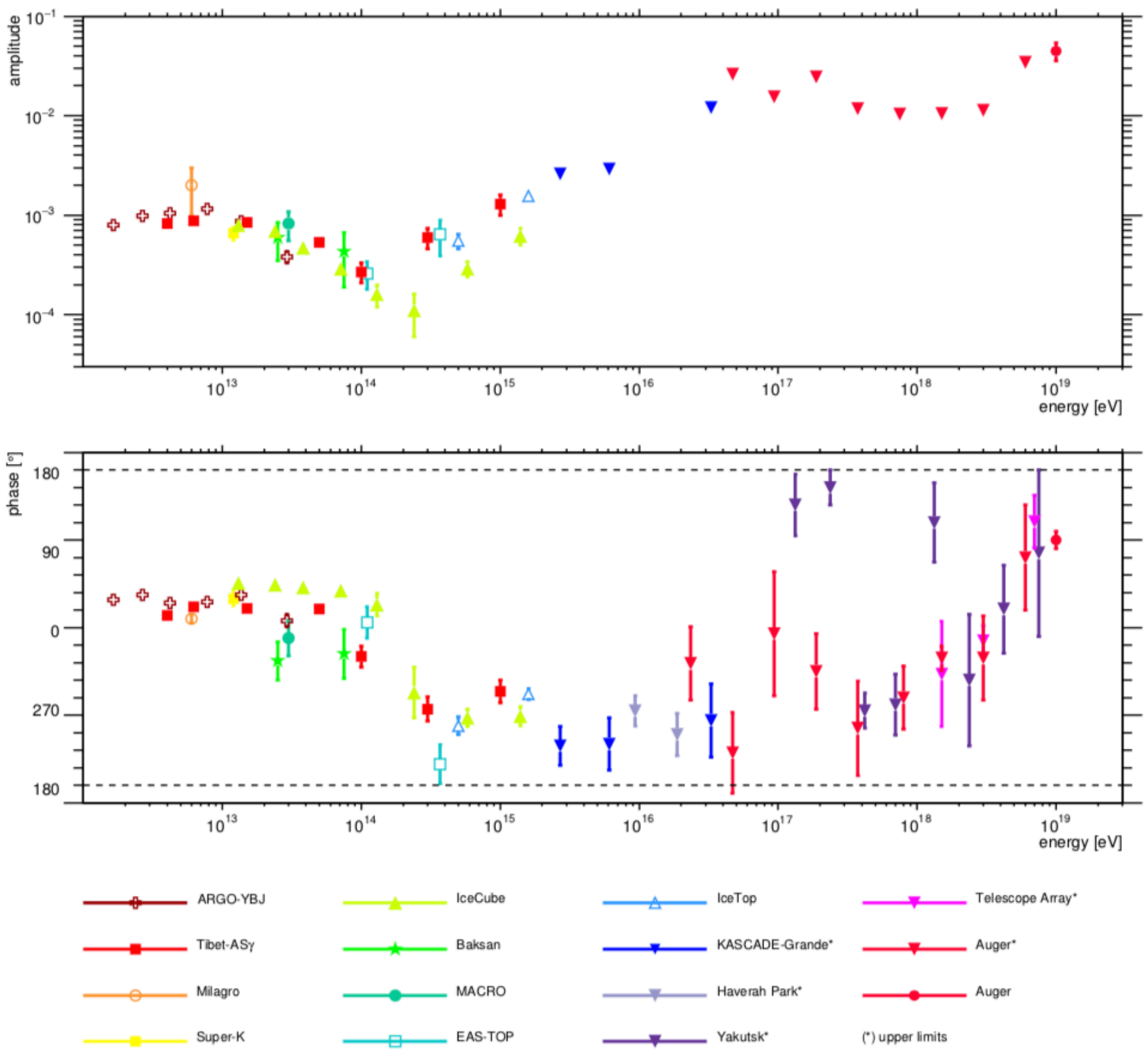

Figure 7: Amplitude (top) and phase (bottom) measurements of the first harmonic in right ascension as a function of energy, from various reports. Amplitudes drawn as triangles with apex pointing down are the most stringent upper limits up to date in the considered energy ranges.

Amplitude and phase of dipole as function of energy

O. Deligny, arXiv:1808.03940

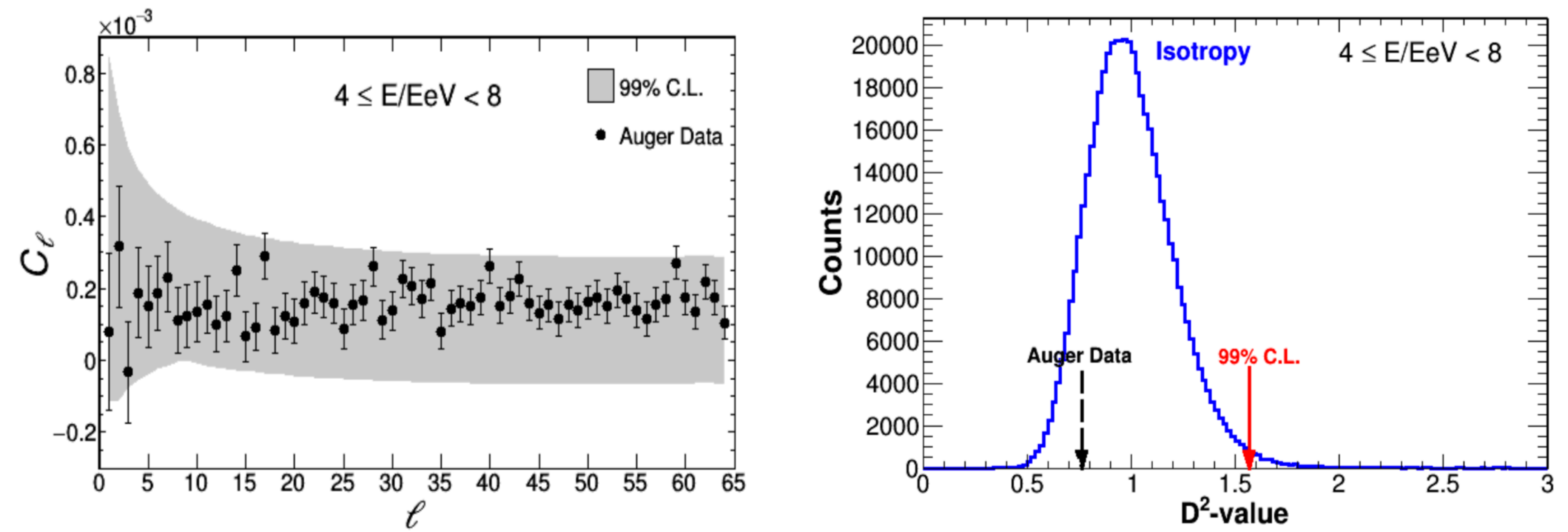

Figure 2: Angular power spectrum for $4 \leq E/\mathrm{EeV} < 8$. On the left there is no visible departure from the isotropic expectation. On the right the D^2-value distribution from 500,000 isotropic sky maps is shown. The red arrow represents the threshold to accept/reject the isotropy hypothesis with 99% C.L.. The D^2-value from data, represented by the black (dashed) arrow, is smaller than that threshold supporting the isotropy hypothesis.

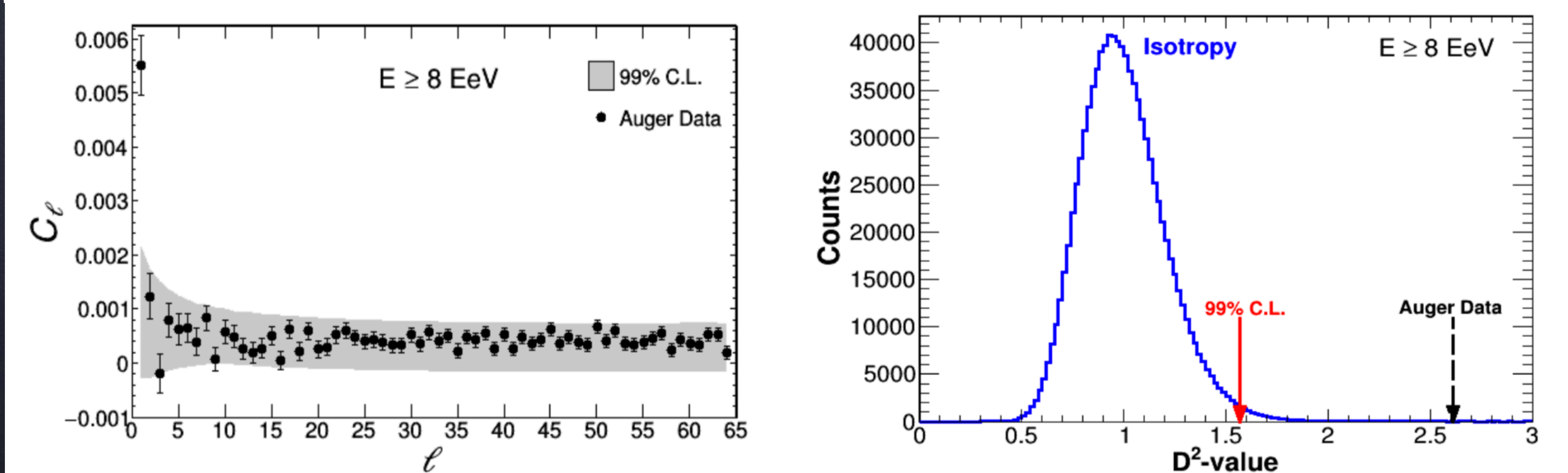

Figure 3: Angular power spectrum for $E \geq 8$ EeV. On the left a clear indication for a departure from isotropy is captured in the dipole scale. On the right the D^2-value distribution from 1,000,000 isotropic sky maps is shown. The D^2-value from data, represented by the black (dashed) arrow, is larger than the threshold of isotropy presenting an indication of anisotropy with $> 99\%$ C.L..

higher order multipoles will become more important to model

Pierre Auger collaboration, JCAP 1706 (2017) no.06, 026 [arXiv:1611.06812]

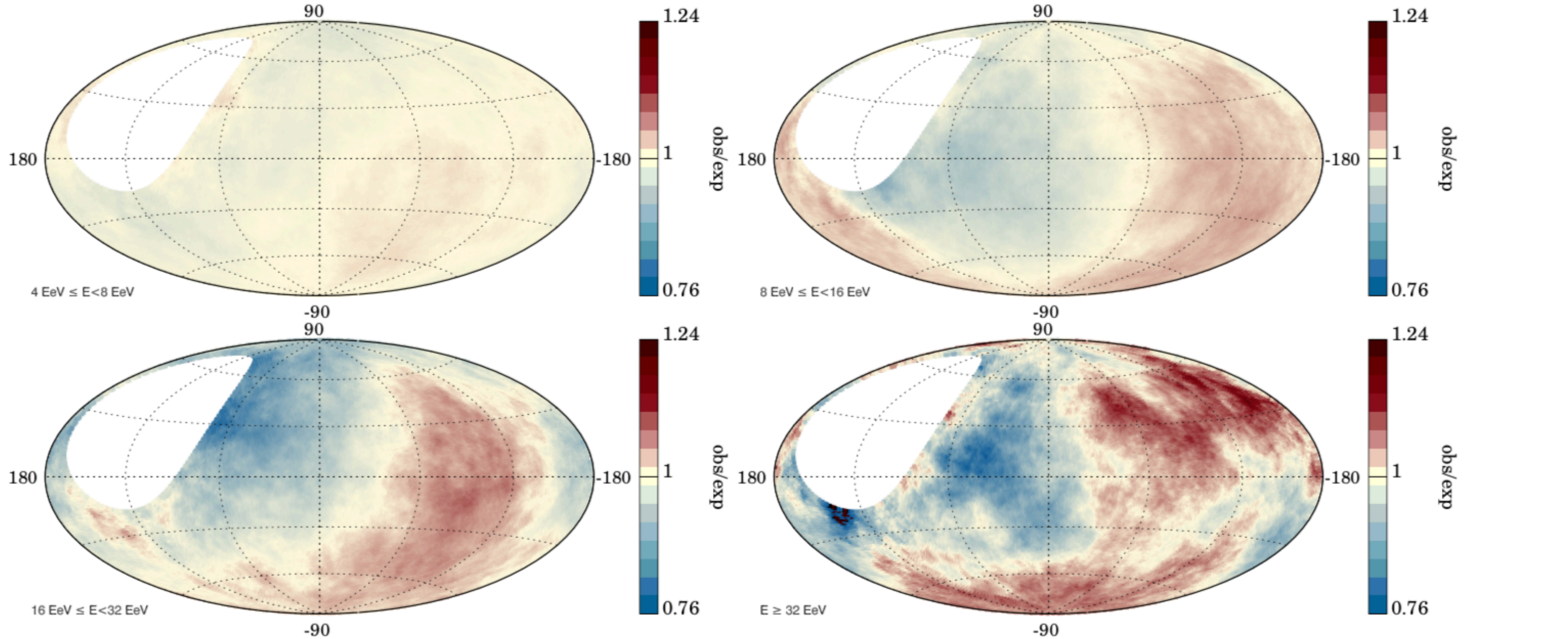

Figure 4. Maps in Galactic coordinates of the ratio between the number of observed events in windows of 45° over those expected for an isotropic distribution of arrival directions, for the four energy bins above 4 EeV.

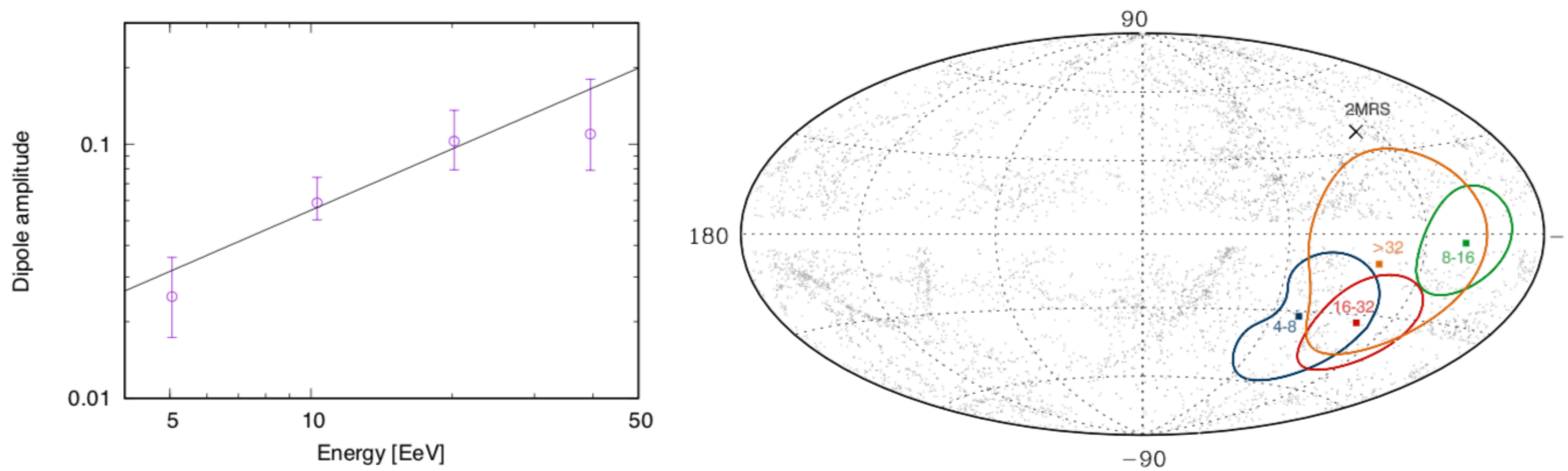

Figure 3. Evolution with energy of the amplitude (left panel) and direction (right panel) of the three-dimensional dipole determined in different energy bins above 4 EeV. In the sky map in Galactic coordinates of the right panel the dots represent the direction towards the galaxies in the 2MRS catalog that lie within 100 Mpc and the cross indicates the direction towards the flux-weighted dipole inferred from that catalog.

Pierre Auger collaboration, arXiv:1808.03579

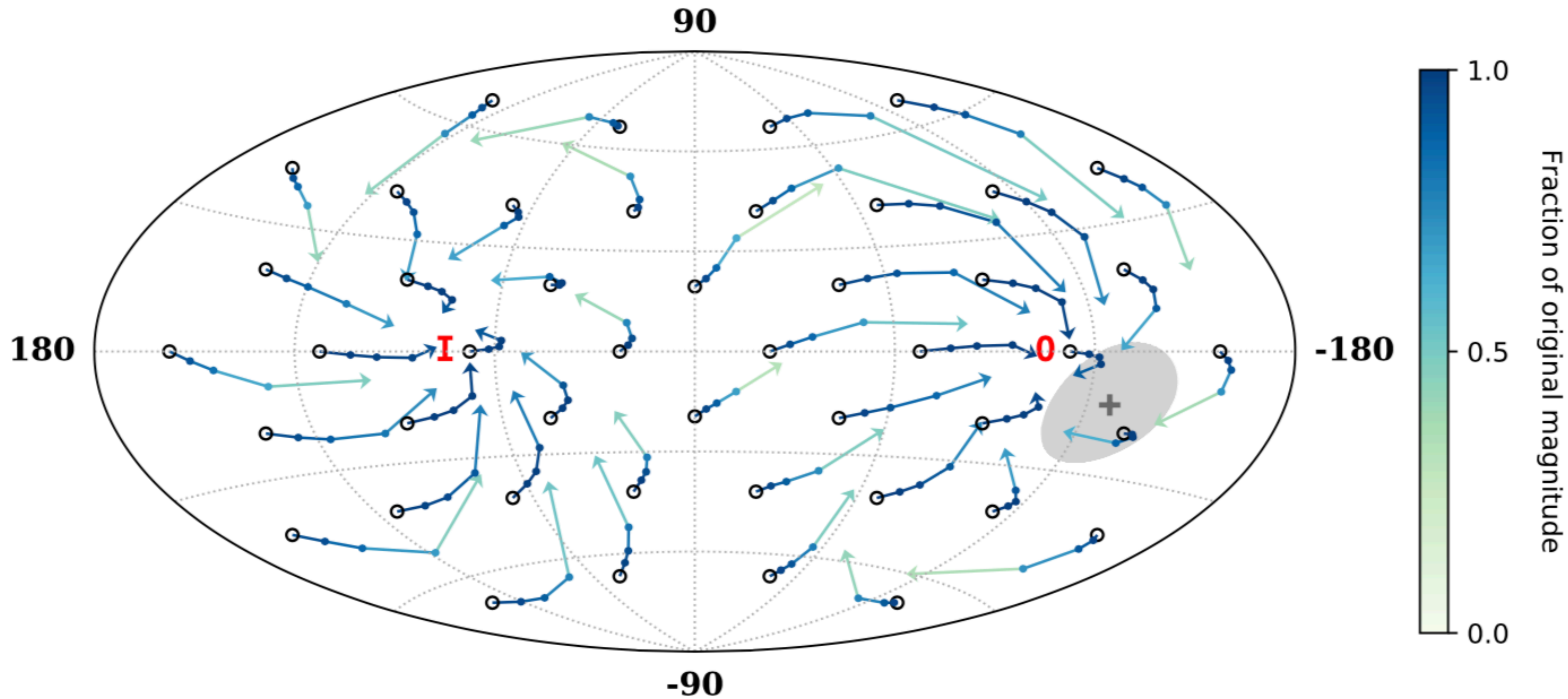

Figure 7. Change of the direction of the dipolar component of an extragalactic flux after traversing the Galactic magnetic field, modeled as in Jansson & Farrar (2012). We consider a grid (black circles) corresponding to the directions of a purely dipolar flux outside the Galaxy. Points along the lines indicate the reconstructed directions for different values of the particle rigidity: 32 EV, 16 EV, 8 EV and, at the tip of the arrow, 4 EV, respectively. The line color indicates the resulting fractional change of the dipole amplitude. The observed direction of the dipole for energies $E \geq 8$ EeV is indicated by the gray cross, with the shaded area indicating the 68% CL region. The labels **I** and **O** indicate the directions towards the inner and outer spiral arms, respectively.

Pierre Auger collaboration, arXiv:1808.03579

Hot spot

E>57 EeV - Years 1-9 excess map

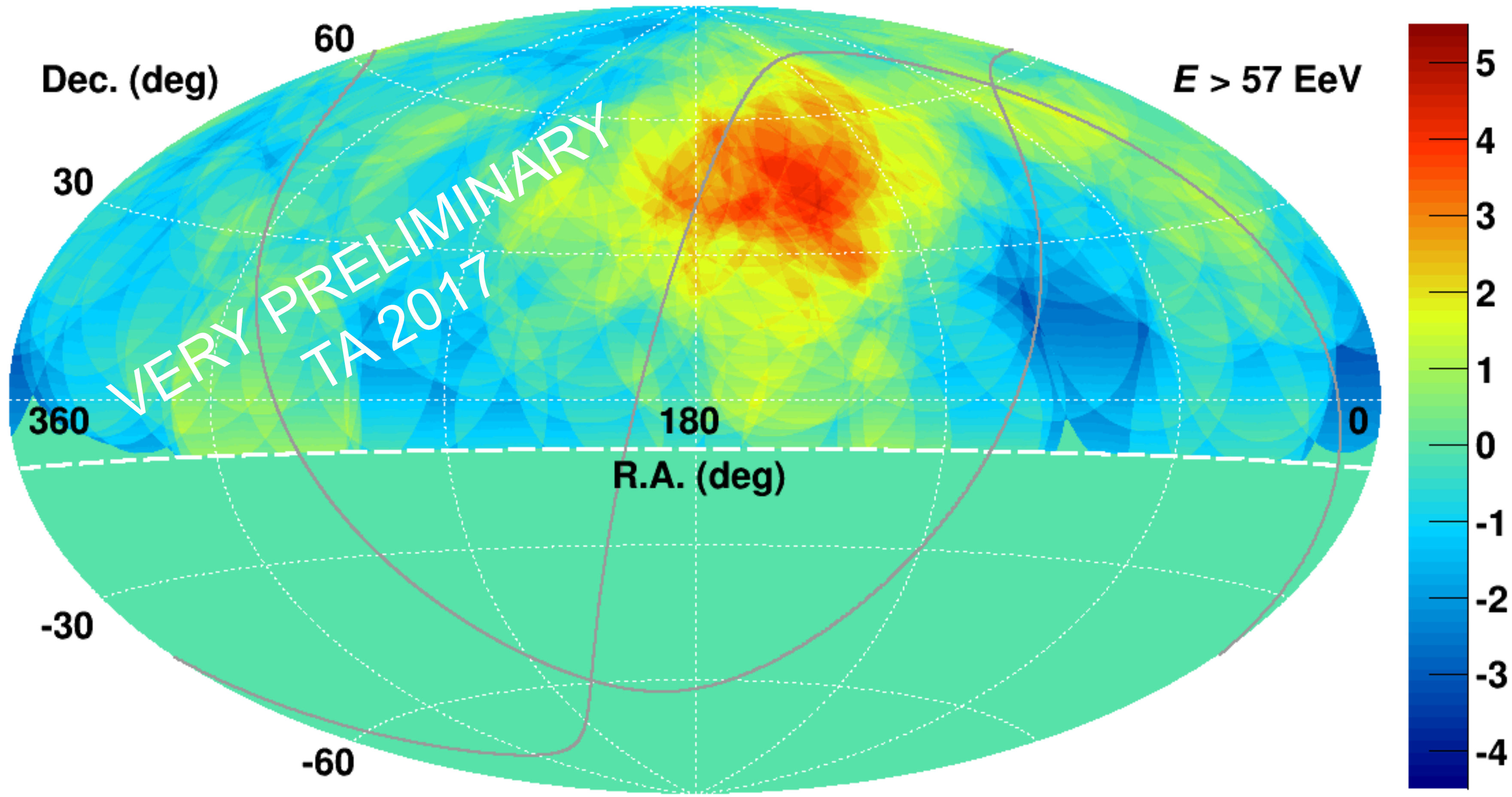

Total events: 143
Observed: 34
Expected : 13.5

Best circle center: RA=144.3°, Dec=+40.3°
Best circle radius: 25°
Local significance : 5 σ
Global significance : 3 σ

TA 2017

Modelling Cosmic Rays in the Structured Universe

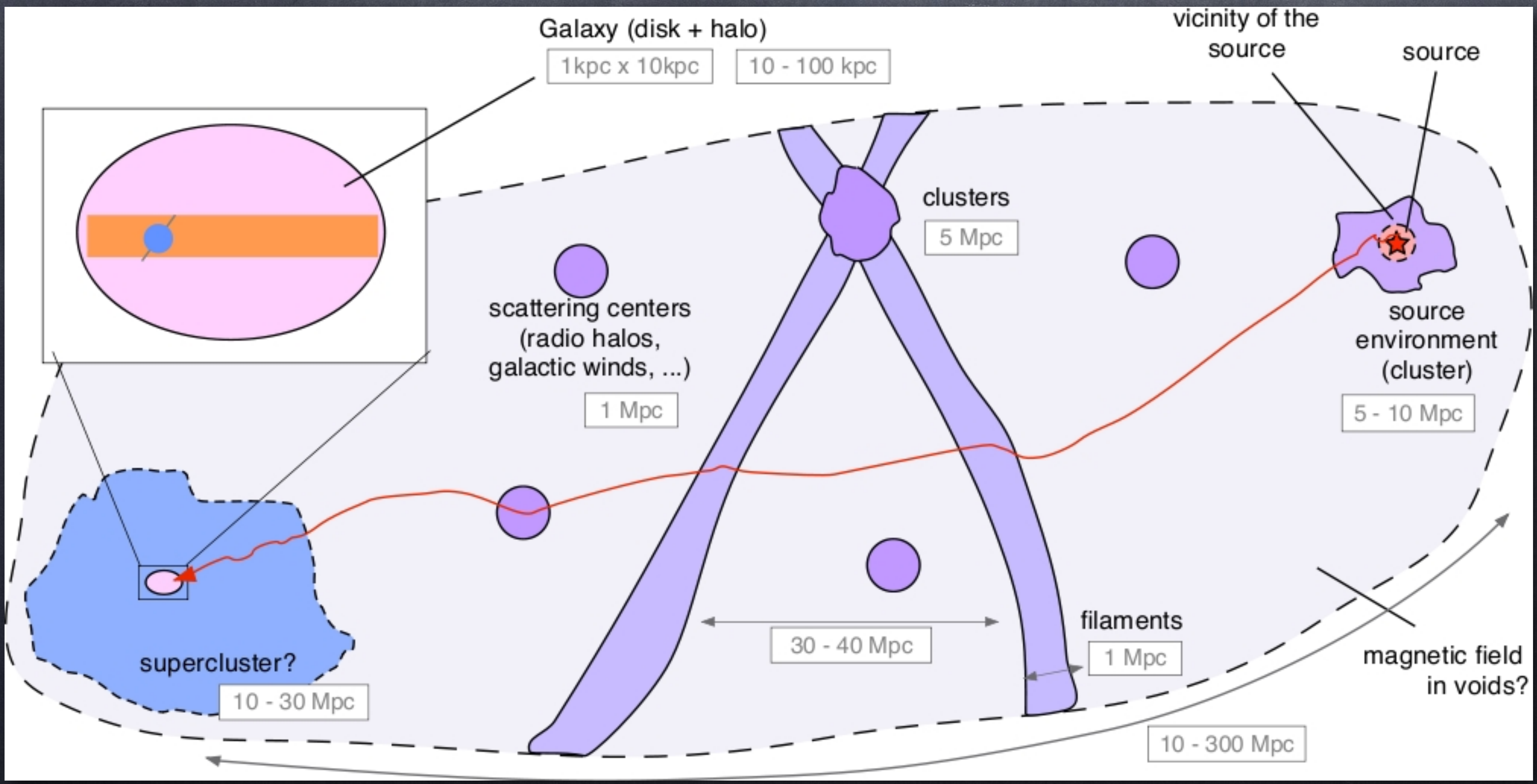

Kotera, Olinto, Ann.Rev.Astron.Astrophys. 49 (2011) 119

Modelling Challenges

- Broad dynamic range in length and time scales
- partly unknown propagation mode: ballistic versus diffusive
- disentangling source distribution/rates from propagation mode

Reminder: Propagation Theorem/Liouville Theorem

A homogeneous distribution of sources with equal properties and nearest neighbour distances smaller than other relevant length scales in the problem such as energy loss length and propagation/diffusion length within the source activity time scale gives rise to a universal/isotropic flux spectrum that does not depend on the propagation mode and thus on the magnetic field properties.

Easiest to see in the back-tracking picture:

The differential flux in the direction characterised by the unit vector $\mathbf{n}$ at observer position $\mathbf{r}_0$ is given by

$$j(E_0, \mathbf{r}_0, \mathbf{n}) = \int_{t_0}^{t_{\max}} dt \dot{\rho} \left[E(t), t, \mathbf{r}(t, \mathbf{n})\right] \, ,$$

where $\dot{\rho}(E, t, \mathbf{r})$ is the differential injection rate at energy E, time t, and location $\mathbf{r}$, $\mathbf{r}(t, \mathbf{n})$ is the back-tracked trajectory with the initial conditions $\mathbf{r}(t_0, \mathbf{n}) = \mathbf{r}_0$, $\dot{\mathbf{r}}(t_0, \mathbf{n}) = \mathbf{n}$ and $E(t)$ with $E(t_0) = E_0$ is the back-tracked energy. For stochastic losses one has to average over trajectories with equal initial conditions.

Clearly, if $\dot{\rho}$ only depends on E and t, then the flux neither depends on the shape of the trajectories nor on direction, but only on energy, and thus is universal.

This also applies to secondary fluxes such as neutrinos and gamma-rays because densities only depend on the time-integrated interaction rates (and energy loss rates) which are location independent

Corollary:

To be sensitive to the propagation mode, magnetic field structure etc. requires discrete, inhomogeneous source distributions with nearest-neighbour distances larger than energy loss length and/or propagation distance within source activity time

A Simple One Source + Isotropic Background Model

Contribution of the one discrete source to the total flux parametrised by η and deflection spread by concentration parameter κ: Dipole and quadrupole can fix both parameters, e.g. C_2/C_1 fixes κ

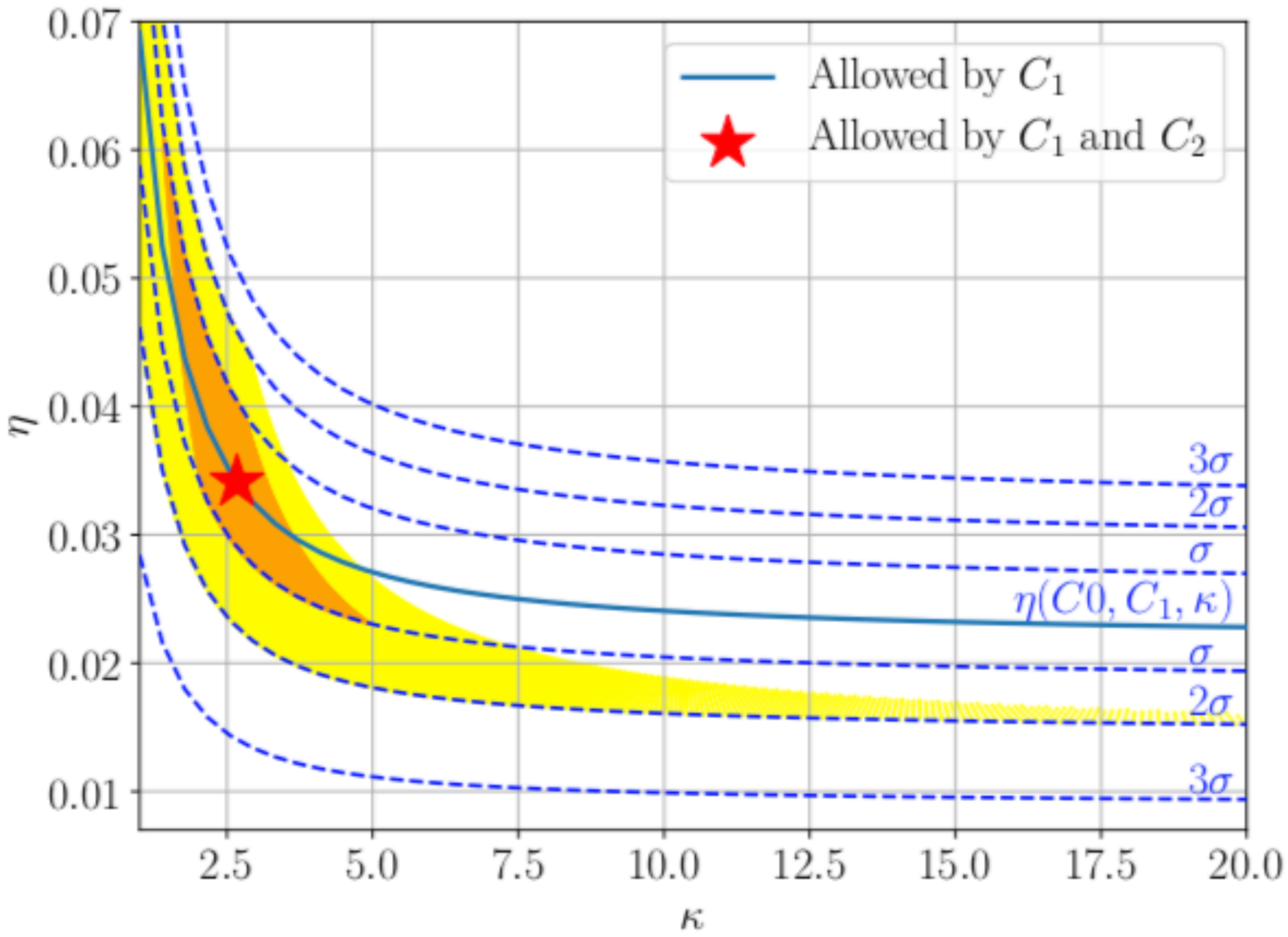

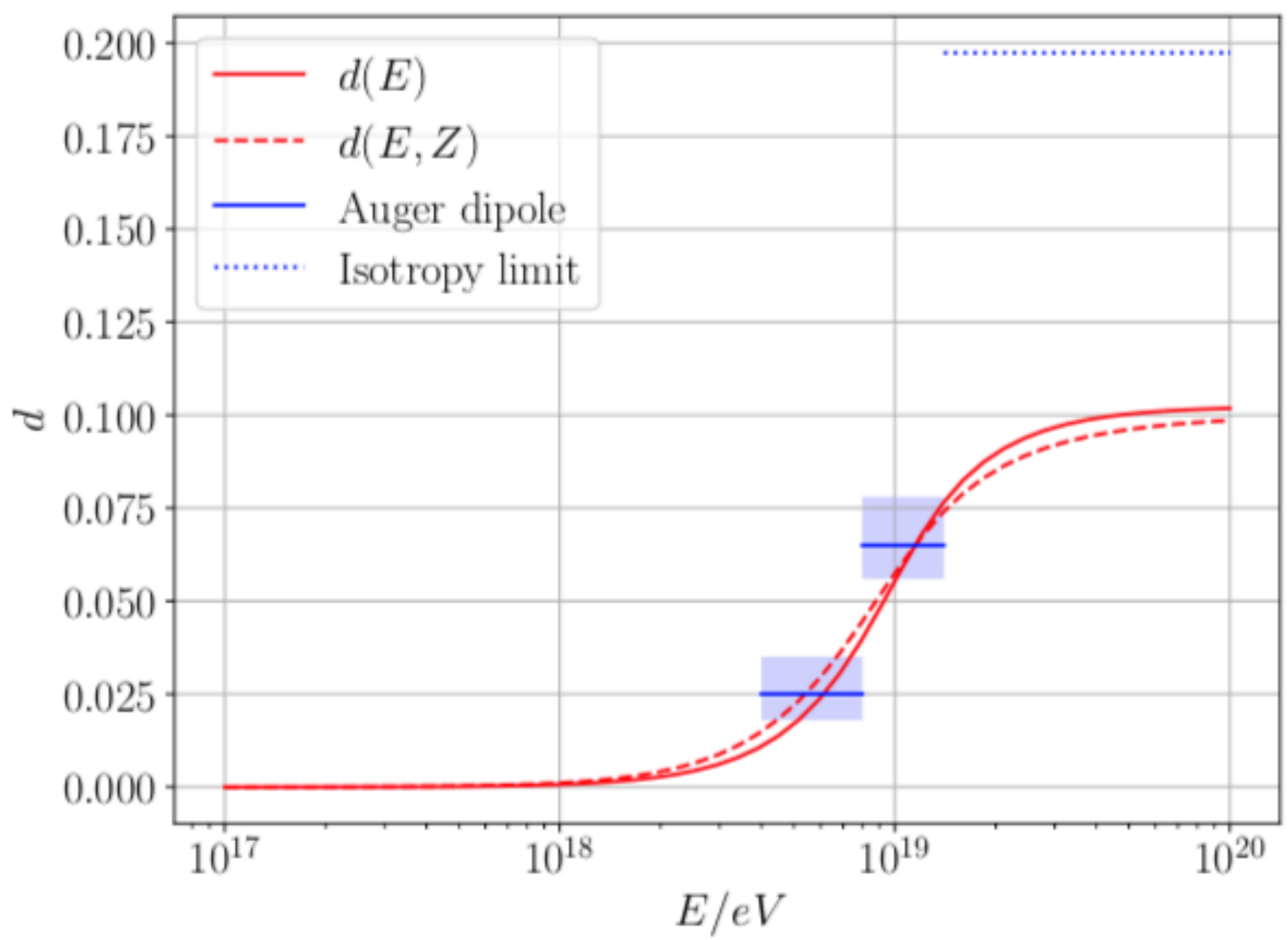

Dundovic and Sigl, arXiv:1710.05517

Dundovic and Sigl, arXiv:1710.05517

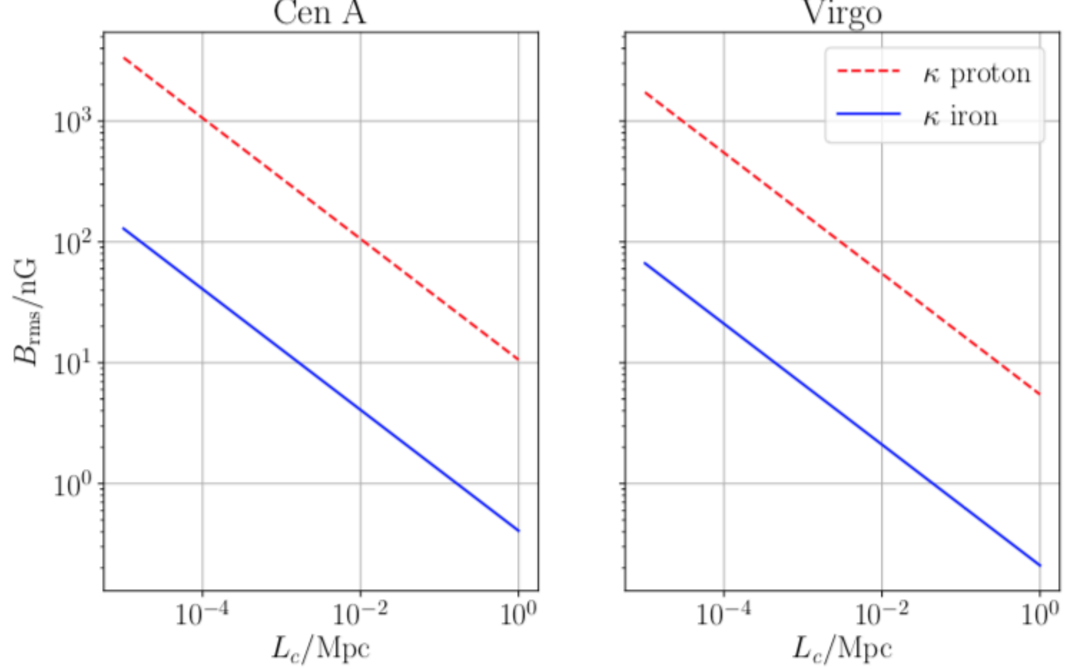

Figure 12. For a source of a given distance, the remaining parameters left undetermined are charge, magnetic field strength and coherence length. The plot shows the relation between $B_{\rm rms}$ and L_c following from eq. 3.4 for the fitted value of κ, for proton and iron primaries coming from Centaurus A and the Virgo cluster.

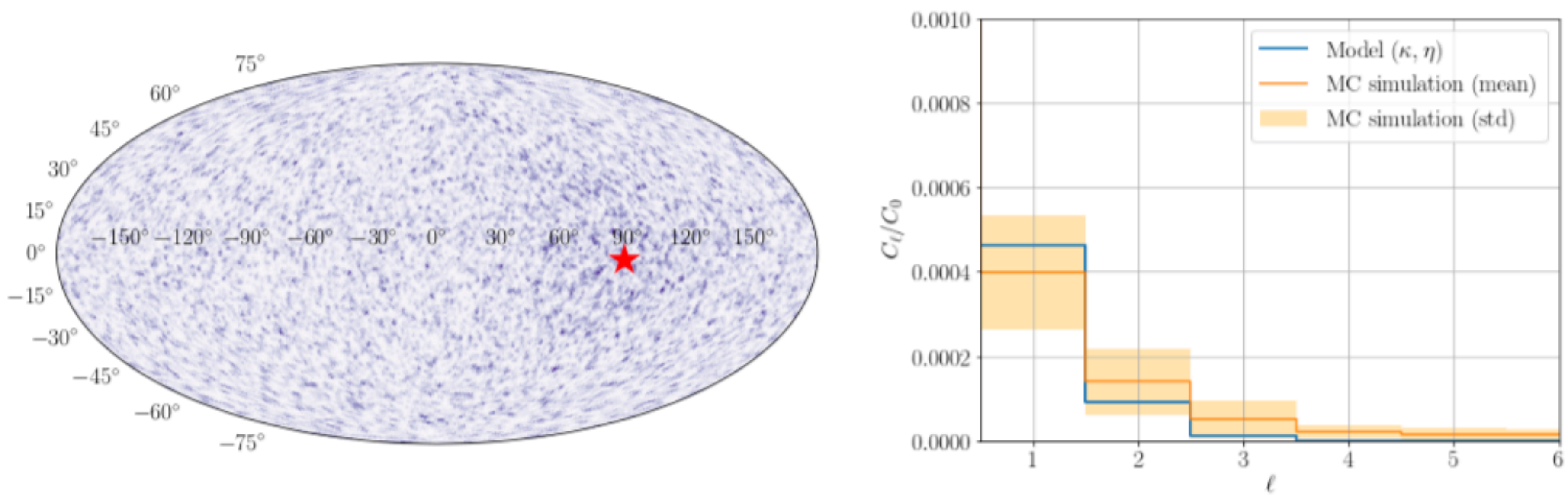

Figure 13. The two plots are results of a Monte Carlo simulation which is set up as described in the text. The sky plot shows the dipole induced by the single source which is placed at 4 Mpc distance from the observer. The direction of the dipole is marked with the star. Other parameters are $Z = 26$, $E = 11.5EeV$, $B_{\rm rms} = 2.9\,{\rm nG}$, $L_c = 30\,{\rm kpc}$, $\eta = 0.03$ where $(1 - \eta)$ is the isotropic contribution from the background. The right panel plot depicts the first few moments of the angular power spectrum where the blue line is the analytically calculated spectrum by using the spread parameter (κ) and the relative flux (η), while the orange line is a fit from the simulation. The orange shaded area represents one sigma fluctuations.

Discrete Sources in nearby large scale structure and structured magnetic field

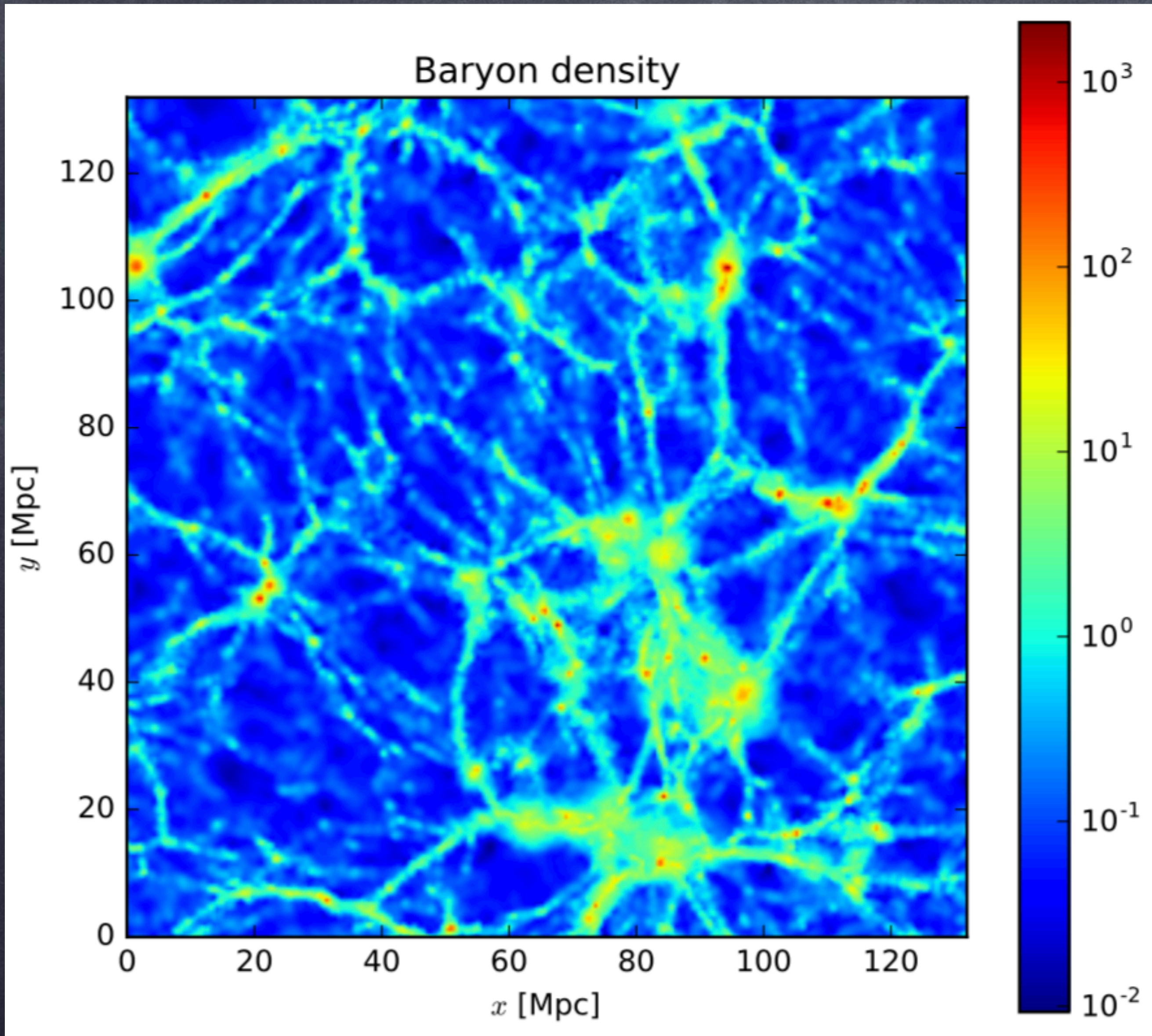

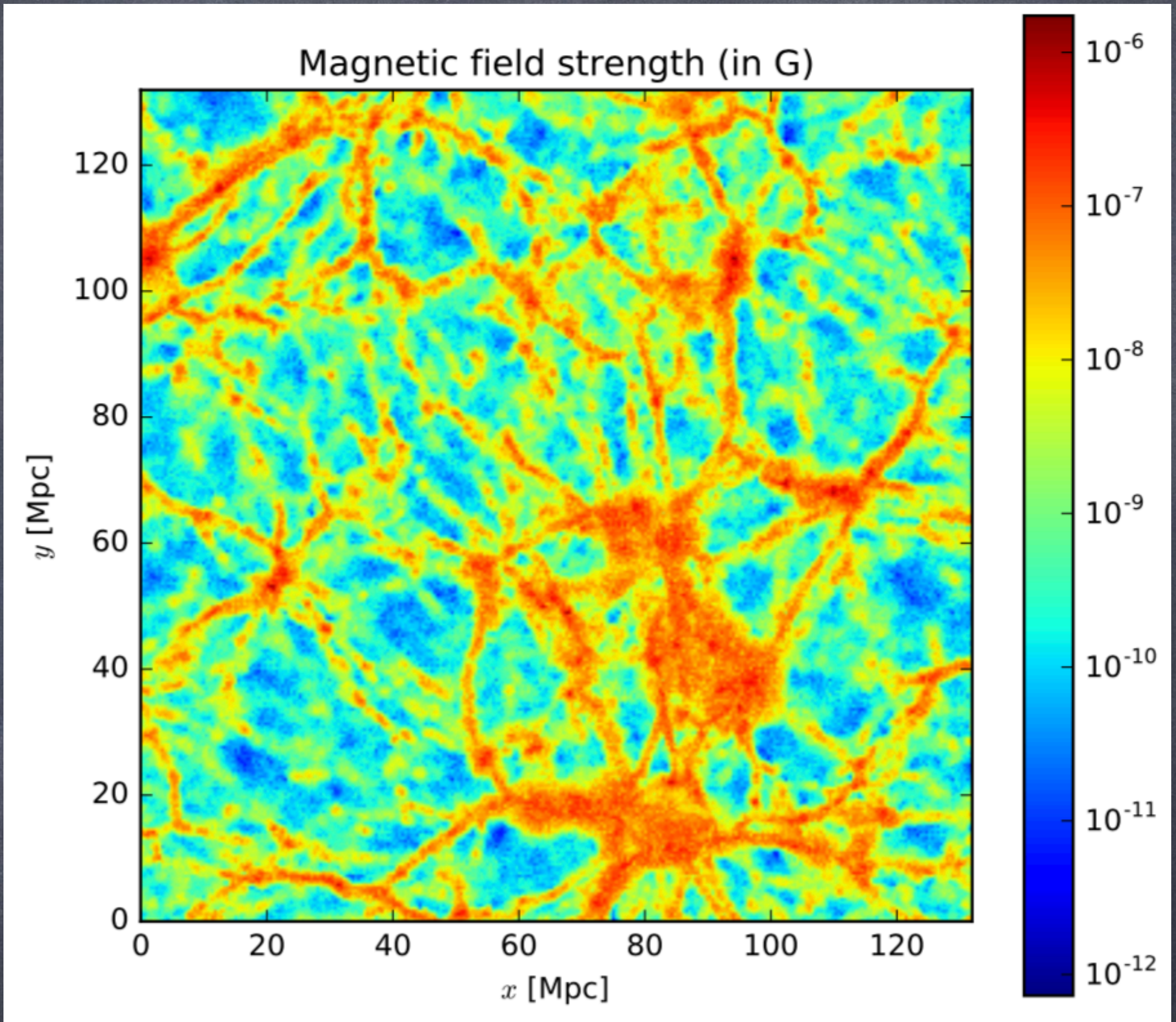

Challenge: Unconstrained/constrained large scale structure simulations often have too limited spatial extent to cover all relevant sources below the GZK energy. Can be partly cured by period boundary conditions which can , however cause artificial regularities in simulated sky maps for small deflections (as can source distributions centered on Earth)

Building Benchmark Scenarios

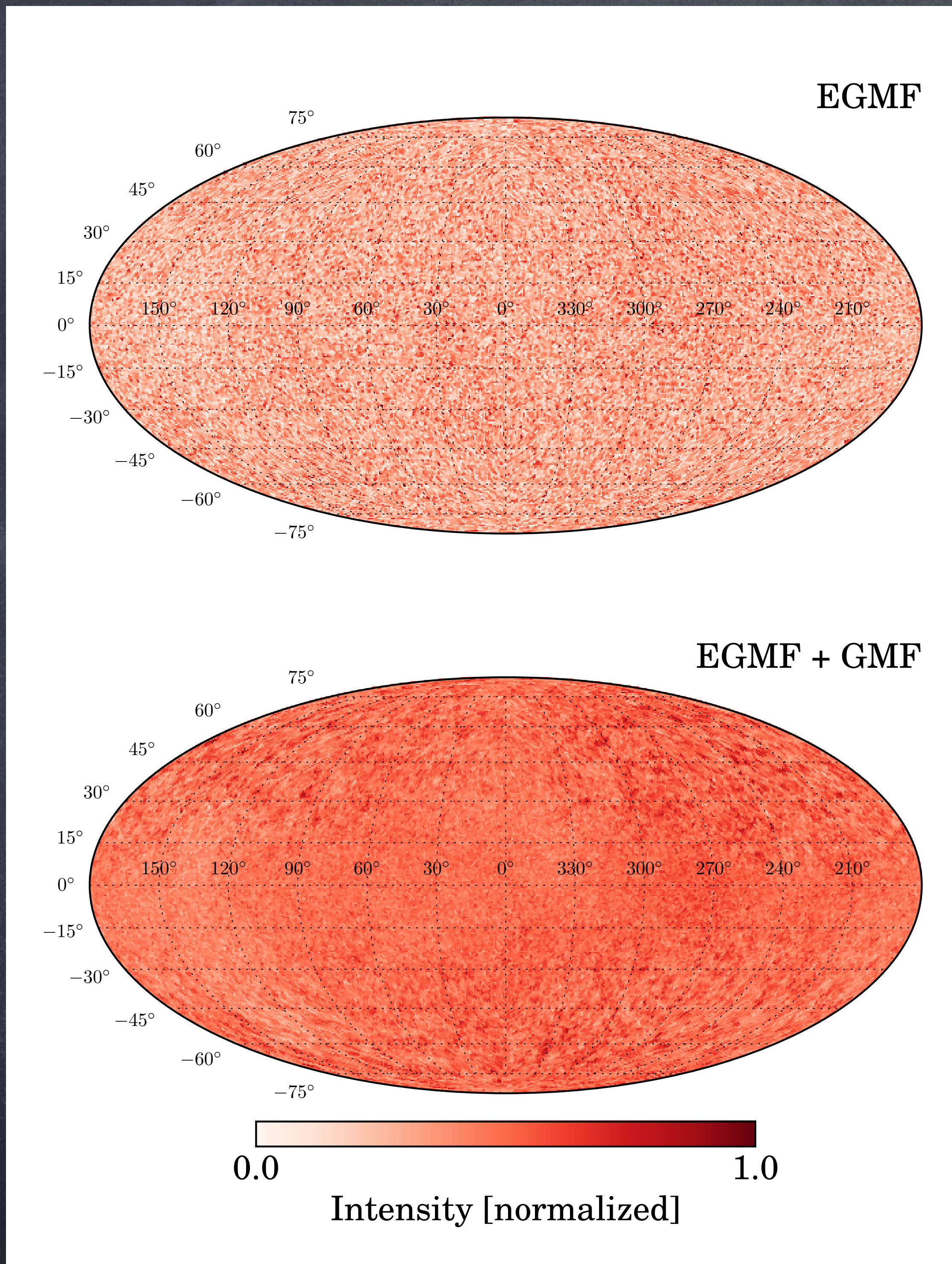

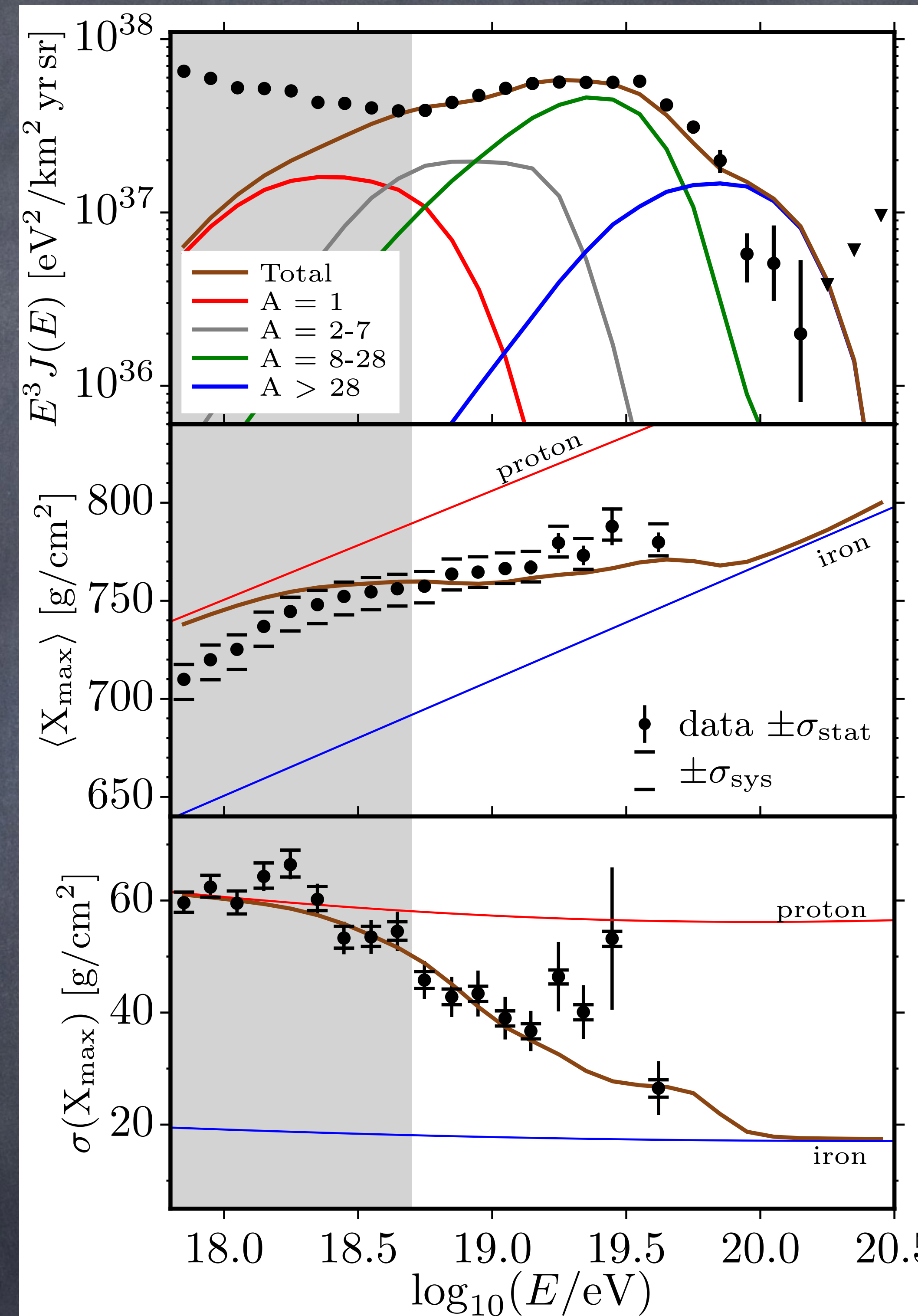

combining spectral and composition information with anisotropy can considerably strengthen constraints on source characteristics, distributions and magnetization

G. Sigl, book "Astroparticle Physics: Theory and Phenomenology", Atlantis Press/Springer 2016, based on David Walz, Pierre Auger collaboration

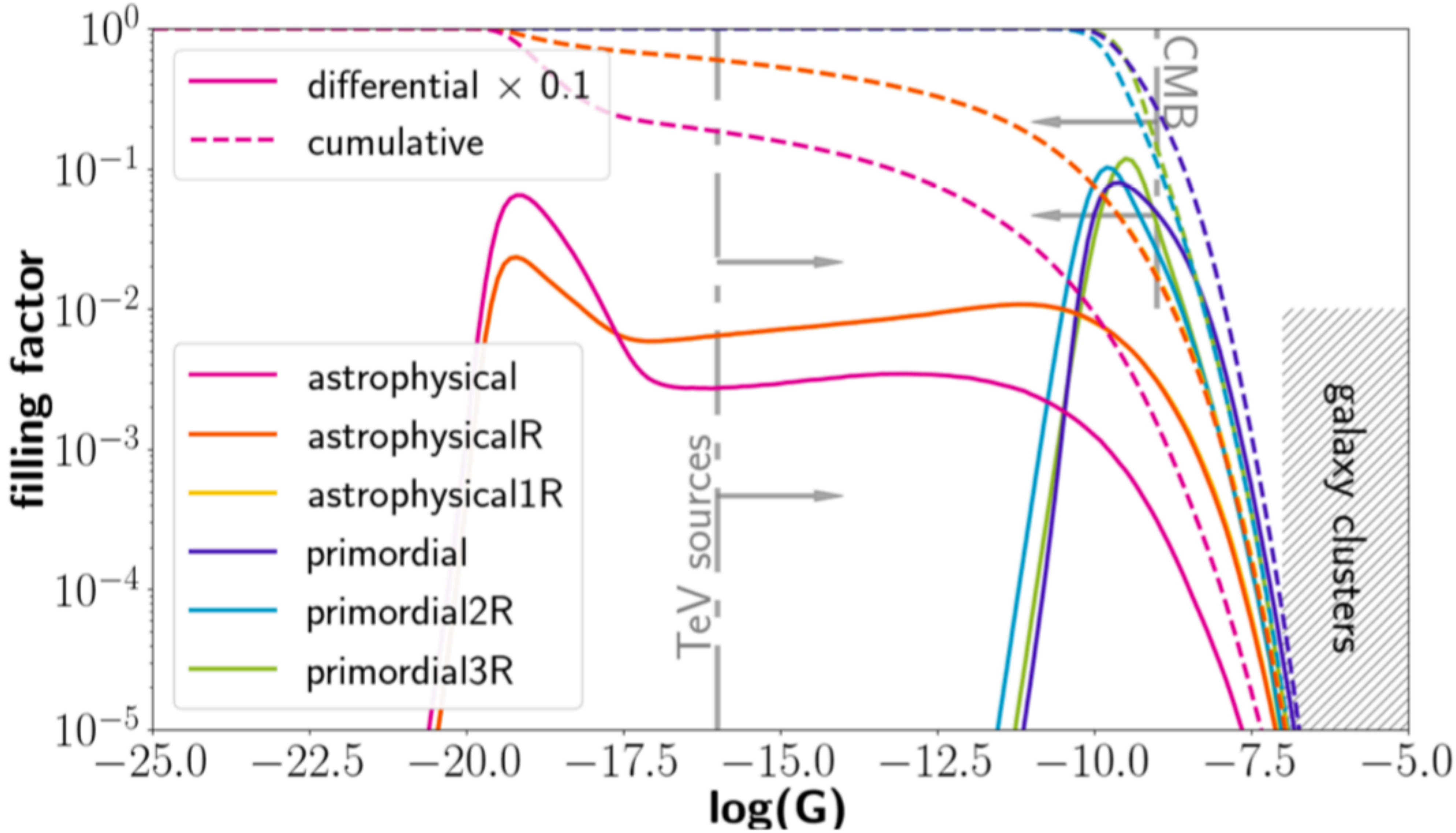

Figure 2. Volume filling factor of the models listed in Tab. 1. The solid lines show the differential filling factor renormalized by 0.1 for clarity, dashed lines show the cumulative filling factor. The grey arrows and shaded area indicate the limits given from observations as listed in the introduction. The yellow line of the *astrophysical1R* model fits exactly with the *astrophysicalR* model.

Hackstein et al., Mon.Not.Roy.Astron.Soc. 475 (2018) no.2, 2519 [arXiv:1710.01353]

Simulated Predictions of angular Multipoles

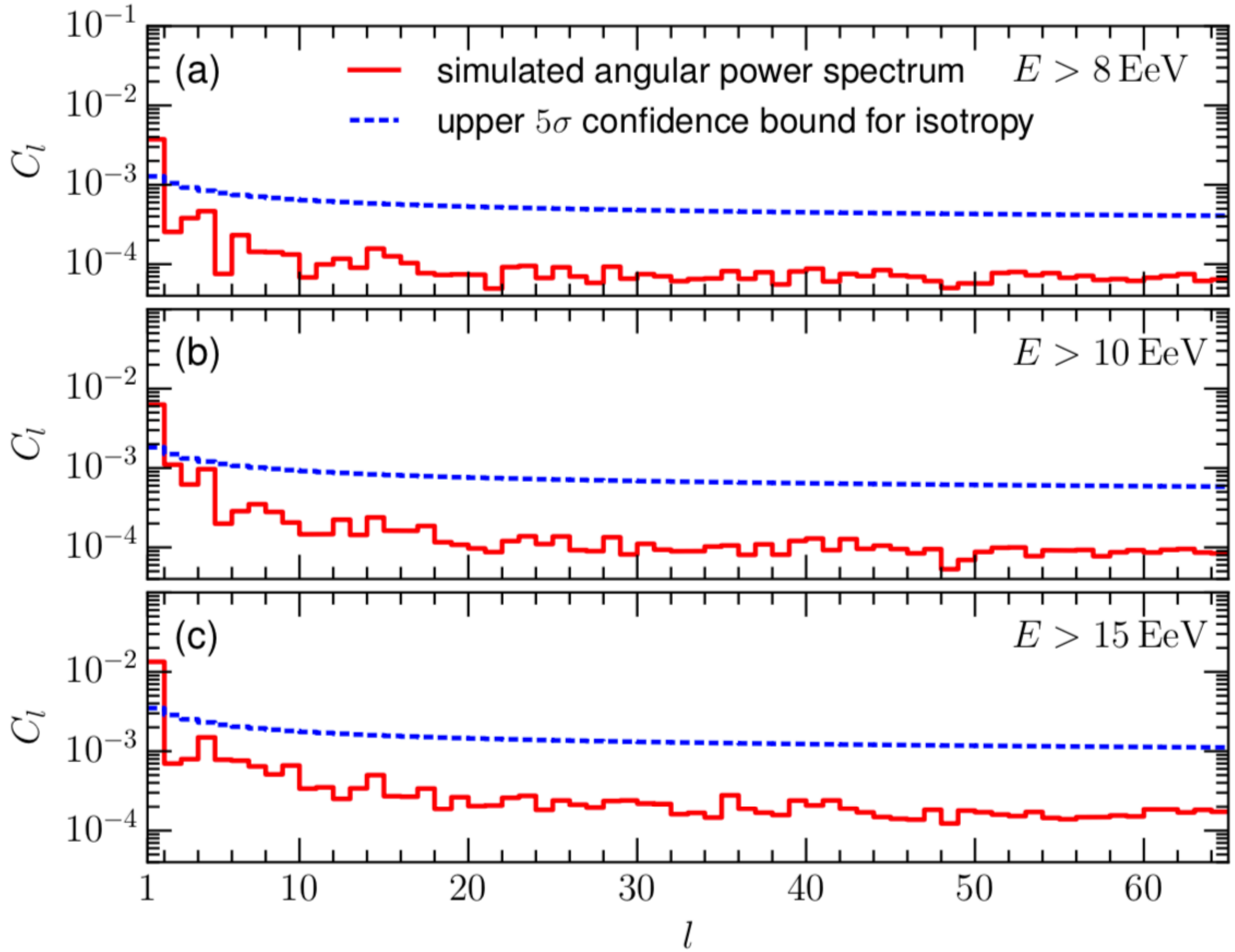

Figure 1. Angular power spectrum (solid red curves) for the arrival directions of the simulated UHECR reaching the observer with energies (a) $E > 8\,\mathrm{EeV}$, (b) $E > 10\,\mathrm{EeV}$, and (c) $E > 15\,\mathrm{EeV}$ as well as the corresponding upper 5σ confidence bounds for isotropy (dashed blue curves). For all energy intervals there is a significant dipolar anisotropy (see the values of $C_1(E)$), whereas the higher-order $C_l(E)$ are compatible with isotropy.

Wittkowski, Kampert, Astrophys. J. 854 (2018) L3 [arXiv:1710.05617]

based on the "benchmark model" which combines constrained large scale structure simulation with magnetic field strength distribution of Miniati model

inclusion of EGMF also leads to softer best fir injection indices γ ~ 1.6 [Wittkowski, proceedings of ICRC 2017]

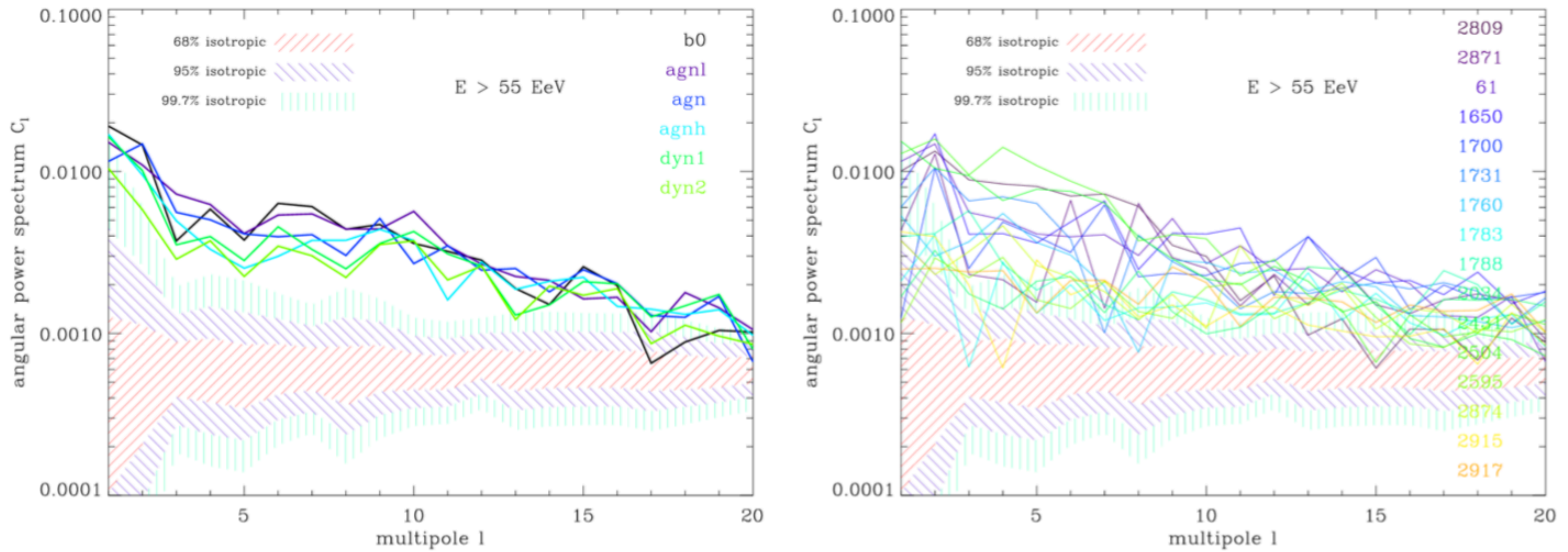

Figure 9. Left: Angular power spectrum of UHECR events observed by ID61 with energies $E > 55$ EeV for the different magnetic field models. Right: same as left, all 16 observers in one model (*agn*).

based on ENZO simulations

Hackstein, Vazza, Brüggen, Sigl, Dundovic,
Mon.Not.Roy.Astron.Soc. 462 (2016) no.4, 3660 [arXiv:1607.08872]

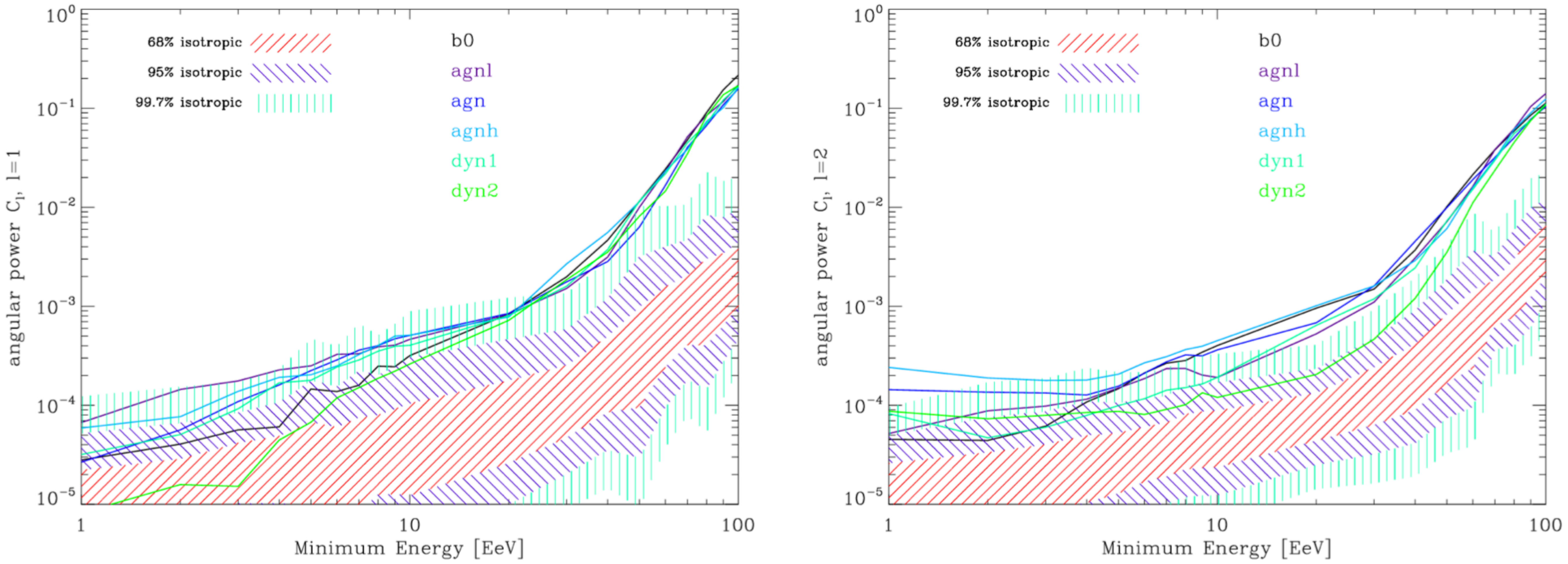

Figure 10. Angular power for the first two multipoles as function of minimum energy of UHECR events observed by ID61.

based on ENZO simulations

Hackstein, Vazza, Brüggen, Sigl, Dundovic,
Mon.Not.Roy.Astron.Soc. 462 (2016) no.4, 3660 [arXiv:1607.08872]

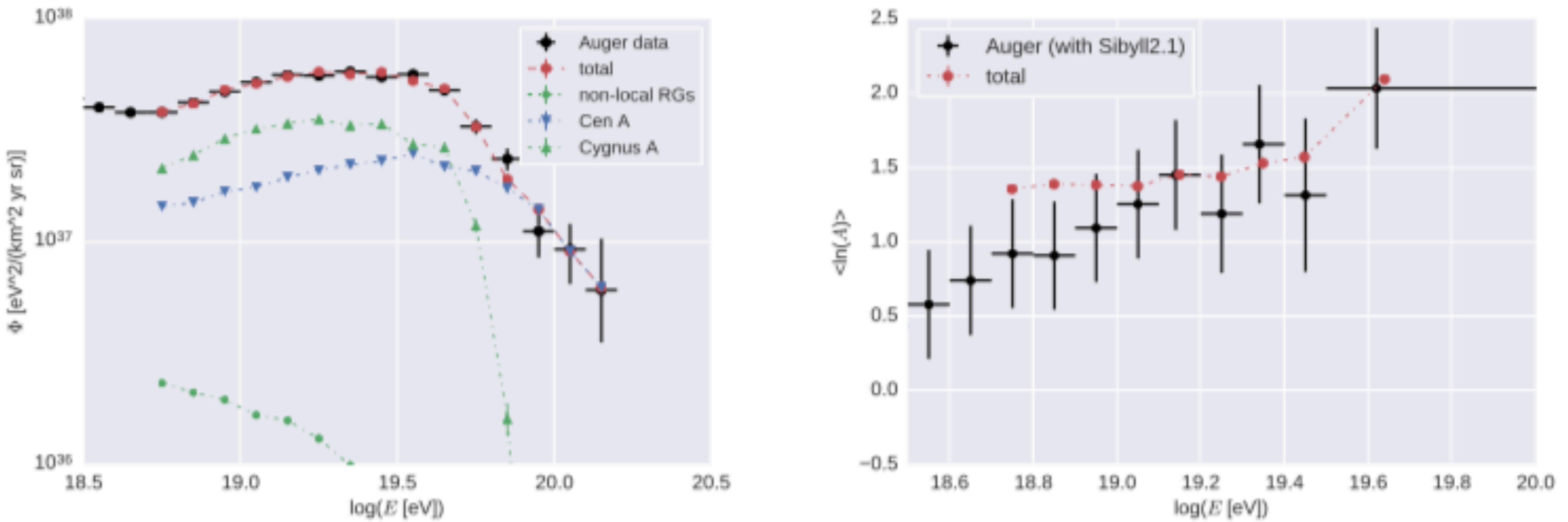

Figure 11. Best-fit results to energy spectrum (left) and chemical composition (right) using Sibyll2.1 and the heavy composition scenario with powerful Centaurus A.

based on a catalogue of radio galaxies where each source has individual injection parameters based on luminosity etc.

Eichmann et al., JCAP 1802 (2018) 036 [arXiv:1701.06792]

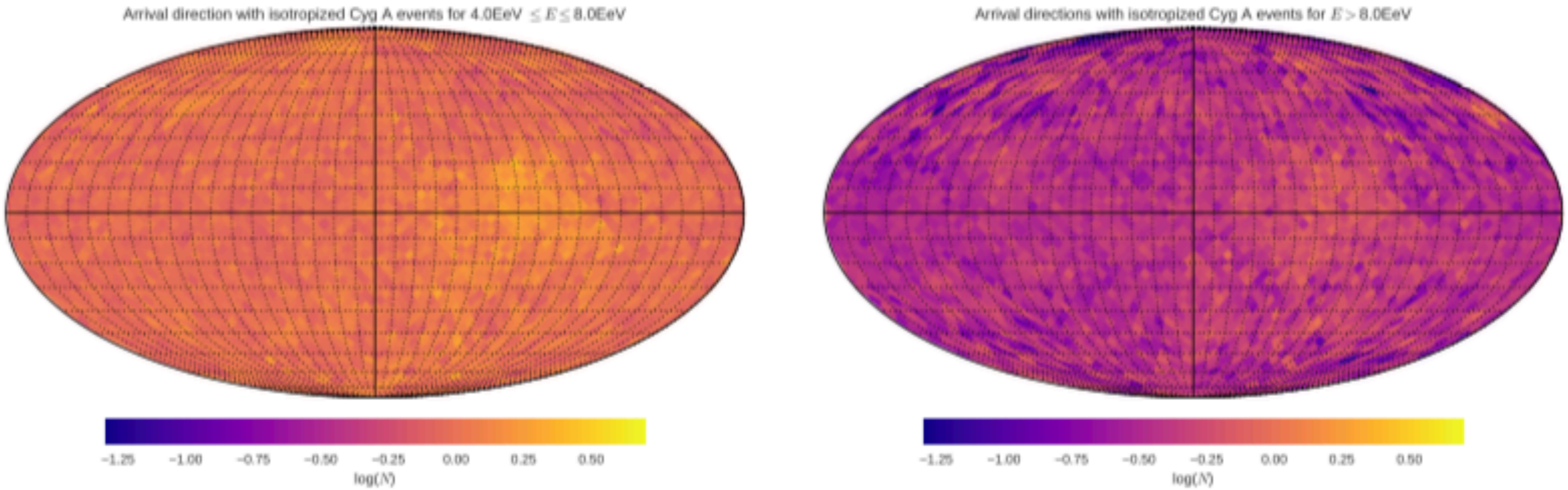

Figure 13. Skymap with isotropized Cygnus A events for $4\,\mathrm{EeV} \leq E \leq 8\,\mathrm{EeV}$ (left), and $E > 8\,\mathrm{EeV}$ (right) using Sibyll2.1 and the light composition scenario with a powerful Centaurus A.

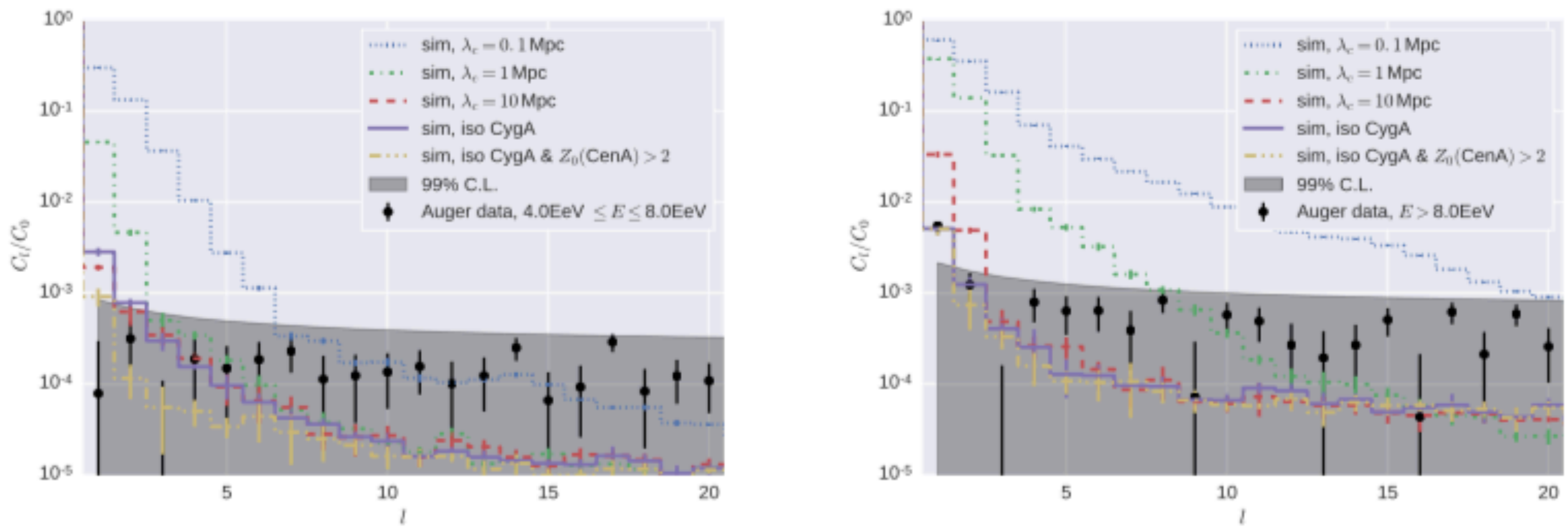

Figure 14. Angular power spectrum with isotropized (solid and dash-dotted line) and non-deflected (dashed line) Cygnus A events for $4\,\mathrm{EeV} \leq E \leq 8\,\mathrm{EeV}$ (left), and $E > 8\,\mathrm{EeV}$ (right) using Sibyll2.1 and the light composition scenario with a powerful Centaurus A.

Eichmann et al., JCAP 1802 (2018) 036 [arXiv:1701.06792]

Many other models have already provided predictions for multipoles/autocorrelations/correlations etc, e.g.

Kalashev, Pshirkov, Zotov, arXiv:1810.02284
Sigl, Miniati, Ensslin, PRD 70, 043007 (2004)

Conclusions

1.) Simulations that simultaneously address spectra, composition and anisotropies/correlations with potential sources become increasingly relevant

2.) Amplitude of anisotropies may be dominated by source distributions/most nearby sources. Magnetic fields may shift directions and mix dipoles; disentangling both influences will be a challenge